HHS Public Access

Author manuscript

Cancer Res. Author manuscript; available in PMC 2025 August 17.

Published in final edited form as:

Cancer Res. 2025 February 17; 85(4): 660–674. doi:10.1158/0008-5472.CAN-24-0456.

HBV Remodels PP2A Complexes to Rewire Kinase Signaling in Hepatocellular Carcinoma

Rigney E Turnham[1,2,*], **Adriana Pitea**[3,*], **Gwendolyn M Jang**[2,4], **Zhong Xu**[5], **Huat Chye Lim**[1,2], **Alex L Choi**[1,2], **John Von Dollen**[2,4], **Rebecca S. Levin**[4], **James T Webber**[5], **Elizabeth McCarthy**[4], **Junjie Hu**[5], **Xiaolei Li**[5], **Li Che**[5], **Ananya Singh**[1,2], **Alex Yoon**[1,2], **Gary Chan**[1,2], **Robin K Kelley**[1], **Danielle L Swaney**[2,4], **Wei Zhang**[3], **Sourav Bandyopadhyay**[5], **Fabian J Theis**[6], **Manon Eckhardt**[2,4,7], **Xin Chen**[5], **Kevan M Shokat**[2,4,8], **Trey Ideker**[3,†], **Nevan J Krogan**[2,4,9,10,†], **John D Gordan**[1,2,†]

[1]Division of Hematology/Oncology, University of California, San Francisco CA

[2]Quantitative Biosciences Institute, University of California, San Francisco CA

[3]Department of Medicine, University of California, San Diego, La Jolla, CA

[4]Department of Cellular and Molecular Pharmacology, University of California, San Francisco CA

[5]Department of Bioengineering, University of California, San Francisco CA

[6]TUM School of Life Sciences, Technical University of Munich, Munich, Germany.

[7]Gladstone Institute of Data Science and Biotechnology, J. David Gladstone Institutes, San Francisco, CA

[8]Howard Hughes Medical Institute, University of California, San Francisco CA

[9]Department of Bioengineering and Therapeutic Sciences, University of California, San Francisco

[10]Gladstone Institute of Data Science and Biotechnology, J. David Gladstone Institutes, San Francisco, CA

Abstract

Hepatitis B virus (HBV) infections promote liver cancer initiation by inducing inflammation and cellular stress. Despite the primarily indirect effect on oncogenesis, HBV is associated with a recurrent genomic phenotype in HCC, suggesting that it impacts the biology of established HCC. Characterization of the interaction of HBV with host proteins and the mechanistic contributions of HBV to HCC initiation and maintenance could provide insights into HCC biology and uncover therapeutic vulnerabilities. Here, we used affinity purification mass spectrometry to comprehensively map a network of 145 physical interactions between HBV and human proteins in hepatocellular carcinoma (HCC). A subset of the host factors targeted by HBV proteins were

[†]To whom correspondence should be addressed: TI: tideker@health.ucsd.edu; NJK: nevan.krogan@ucsf.edu; JDG: john.gordan@ucsf.edu, John Gordan, MD PhD, University of California, San Francisco, 1700 4th Street, San Francisco, CA 94143.

[*]Equal contribution

Author contributions: Concept and design: JDG, ME, TI, NJK, KMS, XC, WZ, SB, RKK, Experiments and procedures: JDG, AP, RET, ME GMJ, ZX, ALC, JVD, RSL, JTW, HCL, EM, JH, XL, LC, AS, ASY, GC, JC, DS, FJT, WZ; Writing of article: JDG, ME, RET, AP

Conflict of Interest: No relevant conflicts of interest.

preferentially mutated in non-HBV-associated HCC, suggesting that their interaction with HBV influences HCC biology. HBV interacted with proteins involved in mRNA splicing, mitogenic signaling, and DNA repair, with the latter set interacting with the HBV oncoprotein X (HBx). HBx remodeled the PP2A phosphatase complex by excluding striatin regulatory subunits from the PP2A holoenzyme, and the HBx effects on PP2A caused Hippo kinase activation. In parallel, HBx activated mTOR complex 2 (mTORC2), which can prevent YAP degradation. mTORC2-mediated upregulation of YAP was observed in human HCC specimens and mouse HCC models and could be targeted with mTOR kinase inhibitors. Thus, HBV interaction with host proteins rewires HCC signaling rather than directly activating mitogenic pathways, provide an alternative paradigm for the cellular effects of a tumor promoting virus.

Significance

Integrative proteomic and genomic analysis of HBV/host interactions illuminated modifiers of hepatocellular carcinoma behavior and key signaling mechanisms in advanced disease, which suggested that HBV may have therapeutically actionable effects.

Keywords

Hepatitis B Virus; Host-virus interactions; systems biology; protein phosphatase 2A; liver cancer

Introduction

Hepatocellular carcinoma (HCC) is a leading cause of cancer death worldwide (1). Comprehensive genomic profiling of HCC has revealed only a low incidence of targetable driver mutations (2,3). Accordingly, HCC treatment is currently directed at common disease features such as angiogenesis or immune evasion (4). Although FGF19 amplification has been validated as a targetable driver in HCC (5), there are currently no molecularly targeted agents in use for HCC and further investigation is required to identify targetable mechanisms of HCC growth.

The majority of HCC arises in the setting of co-morbid hepatitis due to viral infection caused by hepatitis B or hepatitis C viruses (HBV or HCV), or metabolic disorders such as non-alcoholic steatohepatitis (2,3). Some tumor-associated viruses exert direct effects on tumor maintenance, such as the degradation of *TP53* by Human Papilloma Virus (HPV) E6 (6). Hepatitis viruses primarily promote tumor initiation via increased local inflammation and cell turnover (2,3,7). The timeline for HBV- and HCV-induced tumorigenesis in murine models is consistent with an indirect role, with viral proteins causing HCC with >1 year latency (8). In contrast, HPV protein expression causes papillomatosis in mice within 2–3 months (9). Despite its primarily indirect effect on oncogenesis, we and others have identified a recurrent HBV-associated genomic phenotype in HCC (2,3,10) suggesting that it significantly impacts the biology of established HCC.

HBV is a small, enveloped DNA virus which expresses a surface antigen (HBs), core protein (HBc), polymerase (Pol) and a putative oncogenic effector protein, HBV protein X (HBx). Pol is the only HBV protein with enzymatic activity, functioning to initiate minus

strand DNA synthesis and reverse transcribe viral RNA intermediates back into DNA. HBc forms the viral capsid around the HBV genome, with surface antigen mediating hepatocyte binding (7,11). HBx has been ascribed many functions that may promote oncogenesis, including activating the kinase AKT (7). HBx is also necessary for HBV replication based on its ability to hijack the CRL4 E3 ubiquitin ligase (12,13). This effect of HBx has been connected to disrupted DNA-damage repair (14). Earlier, members of this team reported a complete HCV protein-protein interaction (PPI) map (15). In contrast to what is known about HBx, there is no suspected HCV oncogenic effector, and few PPIs are seen with cancer-relevant proteins.

The distinct phenotype of HBV-associated HCC and putative oncogenic effects of HBV proteins motivate further study to characterize HBV's interaction with host proteins and thus its mechanistic contributions to HCC initiation and maintenance. Integrative models of multilevel data are well-suited to study the complex interactions between cancer and infectious diseases. We have previously used a similar approach where we integrated host/HPV PPIs with cervical and oropharyngeal cancer genomics This strategy enabled identification of cancer pathways that are modulated either by HPV in virus-associated tumors or by somatic mutations in non-viral tumors (6). Here, we extend this strategy to HBV and its impact on HCC, further advancing the analytical workflow to address the marked mutational heterogeneity of HCC. This approach yields new insights into HCC biology and demonstrates potent effects of HBV on HCC tumor cell biology, supporting the possibility that HBV infection may result in therapeutic vulnerabilities.

Materials and Methods

Cell culture and treatments

Hep3B (RRID:CVCL_0326), HepG2 (RRID:CVCL_1098), SNU-182 (RRID:CVCL_0090), SNU-387 (RRID:CVCL_0250), SNU-398 (RRID:CVCL_0077), SNU-423 (RRID:CVCL_0366), SNU-449 (RRID:CVCL_0454), SNU-475 (RRID:CVCL_0497), and PLC/PRF/5 (RRID:CVCL_0485) were obtained from ATCC (Manassus, VA). HUH7 (RRID:CVCL_0336) was obtained from the UCSF Cell Culture Facility and HUH6 was obtained from the RIKEN cell bank (Tsukuba, Japan). HLE (RRID:CVCL_1281), HLF (RRID:CVCL_2947), FOCUS (RRID:CVCL_7955) and Hep40 (RRID:CVCL_EI25) were obtained from Dr. Ju-Seog Lee (MD Anderson Cancer Center). MHCC97-H (RRID:CVCL_4972) and MHCC97-L (RRID:CVCL_4973)were obtained from Zhongshan Hospital of Fudan University, Shanghai. Cells were cultured in DMEM with high glucose (Invitrogen, Carlsbad CA) with 10% fetal calf serum (Axenia BioLogIx, Dixon CA) for all experiments, with SNU-182, SNU-387, SNU-398, SNU-423, SNU-449, SNU-475 passaged in RPMI/10% FCS. Puromycin selections were performed at 1 μG/mL and hygromycin selections at 50 μG/mL. Cells were stably maintained in selection conditions. Everolimus, LB-100, MG-132, MK-2206, okadaic acid and TAK-228 and were obtained from Selleckchem (Houston, TX), and E-1035 synthesized following established protocols (16). Cells were maintained for 10 or fewer passages and monitored no less than quarterly for mycoplasma contamination and identity confirmed with STR on receipt if not purchased from ATCC. STR was repeated if changes in morphology or behavior were noted or before

key experiments such as screens. Key cell lines were also confirmed by STR at final submission.

Mouse models

Wild-type (WT) FVB/N mice were obtained from Charles River Laboratories (Wilmington, MA) and *Rictor*$^{fl/fl}$ mice from The Jackson Laboratory (Sacramento, CA). Hydrodynamic injection was performed as previously (17). We injected 60μg pT3-EF1α-Cre or 60μg pT3-EF1α (empty vector control) together with 20μg pT3-EF1α-HA-myr-AKT and 20μg pT2-Caggs-RasV12 to delete *Rictor* while co-expressing AKT and Ras. Mice were housed, fed, and monitored in accord with protocols approved by Institutional Animal Care and Use Committee at the University of California, San Francisco (San Francisco, CA), and were monitored for signs of morbidity.

Gene mutation analysis

To determine which protein coding genes were altered in the LIHC TCGA data set, we used the corresponding mutation data files and copy number calls on gene level provided by the Broad Institute TCGA GDAC. The mutation annotation file comprised 53,777 missense mutations as determined by Mutation Assessor (18) in 14,901 RNAs and 373 patients. We classified genes as altered (Mut) or wild type (WT) as follows: We removed variants classified as [‘Silent’, ‘IGR’, ‘5’UTR’, ‘3’UTR’, ‘5’Flank’, ‘3’Flank’, ‘RNA’, ‘Intron’], yielding 41,263 non-silent mutations across 13,675 genes. Additionally, we considered genes with amplifications or deletions as determined by GISTIC as mutated. Once mutations/CNAs were identified, we intersected them with the protein coding genes included in the ReactomeFI PPI reference network (https://reactome.org/). As a result, we determined m=8,765 protein coding genes altered by either mutations, amplifications or deletions, in a set of n=366 patients. Patients with HBV and HCV co-infection were excluded. For the following analysis, we binarized this information for each gene: [0=WT, 1=Mut].

Differential mutation analysis

To determine the effect of the viral infections on the mutational status of each gene in HCC, we assessed the differential mutation rates at gene level between:

A. HCV(+) and HCV(–) HCC cases.

B. HBV(+) and HBV(–) HCC cases.

For this purpose, we set up to map the inputs $x_{g_{hepB}}$, $x_{g_{hepC}}$ to the output y_g, where $g \in \{g_1, \ldots, g_m\}$. The output y_g is a one dimensional ($1d$) vector of length n representing the mutational status across the n HCC patients for each mutated gene g (0 = wild type; 1 = altered). The features $x_{g_{hepB}}$ and $x_{g_{hepC}}$ are $1d$ binary vectors of length n representing the viral infection status for HCV (1 = HCV(+); 0 = HCV(–)) -- $x_{g_{hepC}}$, and the viral infection status for HBV (1 = HBV(+); 0 = HBV(–)) -- $x_{g_{hepB}}$.

Given the response variable y_g is binary, and we aimed to learn the impact of the viral infections on the mutation status, the first choice to formalize the problem was logistic

regression. However, logistic regression returned perfect separation of the response which is a common problem in small sample size studies and imbalanced data. Perfect separation is accompanied by unstable regression coefficients, and can yield misleading findings. Since our aim was to estimate the risk of a mutation happening due to viral infection, and not to solve a binary classification problem, we used the solution proposed by Gelman et al. to obtain stable regression coefficients (19). Following, we formally defined three Bayesian logistic regression models conditioned by independent Student-t prior distributions on the coefficients for each g out of the m mutated protein coding genes:

$$\pi_{g_{complete}}: p\left(y_g \middle| x_{g_{hepB}}, x_{g_{hepC}}\right)$$

$$\pi_{g_{null_1}}: p\left(y_g \middle| x_{g_{hepC}}\right)$$

$$\pi_{g_{null_2}}: p\left(y_g \middle| x_{g_{hepB}}\right),$$

where $\pi_{g_{complete}}$ is defined by the probability mass function of the output y_g given $x_{g_{hepC}}$ and $x_{g_{hepB}}$, $\pi_{g_{null_1}}$ is defined by the probability mass function of the output y_g given $x_{g_{hepC}}$, and $\pi_{g_{null_2}}$ is defined by the probability mass function of the output y_g given $x_{g_{hepB}}$ only. We used the default Cauchy distribution with mean 0 and prior scale 2.5 -- in the simplest scenario, a longer-tailed version of the distribution attained by assuming one-half additional success and one-half additional failure in a logistic regression.

To examine the impact of HBV infection on mutational status of HCC tumors, we compared the likelihood of the $\pi_{g_{complete}}$ model to the likelihood of each of the two alternative models. Hence, we calculated the deviances between the complete model and each of the two alternative models:

$$D_{g_{hepB}} = -2ln\left(\frac{L_{g_{null1}}}{L_{g_{complete}}}\right)$$

$$D_{g_{hepC}} = -2ln\left(\frac{L_{g_{null2}}}{L_{g_{complete}}}\right)$$

with L being the maximum likelihood, i.e. the probability of the data given the inputs x_g and the parameter vector θ that maximizes $p(y_g|\theta, x_g) = \prod_{i=1}^{n} p(y_{g_i}|\theta, x_{g_i})$, with n representing the number of samples. Our code is available on Github (https://github.com/adspit/HBV_HCC_interaction_inference).

Affinity Purification – Mass Spectrometry:

Affinity purification was performed as previously described (6,20). Briefly, HUH7 cells were transfected with FuGene 6 (Promega, Madison WI), and cell pellets were harvested 40 hours after transfection. Clarified cell lysates were incubated with prewashed Strep-Tactin beads (IBA Life Sciences) and allowed to bind for 2 hours. Following purification, complexes bound to beads were washed and then eluted with desthiobiotin (IBA Life Sciences). Proteins from cell lysates and AP eluates were evaluated by MS as below or separated by SDS-PAGE and either directly stained using the Pierce Silver Stain Kit (Thermo Fisher Scientific) or transferred to a PVDF membrane for immunoblotting.

AP eluates analyzed by MS underwent tryptic digest, desalting, and concentration and were then analyzed by LC/MS-MS on a Thermo Scientific Velos Pro Linear Ion Trap MS system or a Thermo Scientific Q Exactive Hybrid Quadrupole Orbitrap MS system equipped with a Proxeon EASY nLC II high-pressure liquid chromatography and autosampler system. Raw data were searched against SwissProt human protein sequences and the individual viral bait sequences using the Protein Prospector algorithm. PPIs were then scored with MiST algorithm using previously defined conditions (0.309 for reproducibility, 0.75 for specificity, and 0.006 for abundance). Cytoscape was used for visualization of the PPI network (21).

We also performed AP-MS on human bait proteins in the presence or absence of HBx. For these experiments, the bait proteins were cloned into the pcDNA4 vector with an N-terminal 3xFlag tag. These were transfected into HUH7 with pcDNA4-eGFP or pcDNA-ST-HBx, and then AP performed as above, but with anti-Flag-M2 magnetic beads (Sigma Aldrich, St. Louis MO). After washing, enriched proteins were eluted with Flag peptide and then subjected to MS as above. After acquisition, data were again searched against SwissProt human protein sequences. PPIs were scored with the MiST algorithm, as well as Saint (22) and Compass (23). A MiST score of 0.7, Saint BFDR <0.05 and Compass p value < 0.05 were used in combination to define a rigorous set of high-confidence PPIs; these were then overlaid onto the CORUM PPI map to define a strict PPI set. Label free protein quantities were determined for each prey using MaxQuant (24), and statistical inference performed with Ms Stats (25).

Network propagation

We first separately propagated the HBV deviances -- D_{ghepB}, through the reference network. We retained the propagated deviance scores in S_{d_g}. Conceptually, S_{d_g} indicates how likely it is that gene g is affected by proteins with differential viral-associated mutations. Thus, we estimated the viral effect on human proteins within the reference network by scoring the proximity of protein in the reference network to the HBV-interacting proteins at genomic level.

Next, we separately propagated the HBV MiST scores through the reference network. The propagated MiST scores were denoted by S_{p_g}. S_{p_g} represented the likelihood of gene g being affected by proteins that were physically interacting with viral proteins. Thus, we estimated the viral effect on proteins within the reference network, by scoring their proximity to the HBV-interacting proteins at physical level.

For network propagation, we used all human protein coding genes present in the reference network that were also expressed in LIHC (p = 9,803 proteins). Given the topology of the reference network, there are certain nodes (e.g. hubs) which will be 'hot' regardless of the initial scores represented by either deviances or MiST scores. To estimate the expected background of the propagated scores given the network topology, we performed 10,000 permutations in which we randomly reassigned the deviances $D_{g_{hepB}}$, and the HBV MiST scores. To calculate the significance of the propagation score of a specific gene, we ran the network propagation algorithm separately with the permuted deviances and MiST scores as input scores and we calculated empirical *p* values. The *p* values indicated how many times the propagated scores after permutation are greater than the real scores.

We used the gene-wise propagated MiST and deviances scores to calculate a combined measure of significance for each protein coding gene. We defined the combined significance score as:

$$S_{c_g} = S_{d_g} * S_{p_g}.$$

To obtain the null hypothesis distribution of the combined score given the network topology, we performed 10,000 permutations through which we randomly reassigned MiST scores and deviances. We applied the network propagation algorithm and calculated the product of the two propagated scores. We then calculated empirical *p* values corresponding to the combined score. The *p* values indicated which genes had network neighborhoods significantly enriched for both viral interactors and genes with differential mutation rates. We calculated the false discovery rate using the Benjamini–Hochberg procedure (48). The values represented the probabilities of erroneously finding genes with neighborhoods significantly enriched for both viral interactors and genes with differential mutation rates. Next, we used the interactions in the reference network between the proteins that showed combined significance and the viral-host interactions to build integrated interactomes of HBV in HCC (Figure 3C). Our code is available on Github (https://github.com/adspit/HBV_HCC_interaction_inference).

Global phosphoproteomics

Huh7 cells with doxycycline-controlled 3xFLAG-HBx were treated with vehicle or doxycycline for 48 hours. Cells were then harvested in PBS, lysed in lysis buffer (8uM urea, 50mM Tris pH 8, 75mM NaCl, 1X protease and phosphatase inhibitors) and sonicated at 20% for 15 sec. Bicinchoninic acid (BCA) protein assay was performed to quantify protein lysates. Samples were reduced, alkylated and subjected to trypsin digestion at 37C overnight. Phosphopeptide enrichment was performed with immobilized metal affinity chromatography following established protocols (26). Enriched samples were analyzed on a Q Exactive Orbitrap Plus mass spectrometry system (Thermo Fisher Scientific). All mass spectrometry was performed at the Thermo Fisher Scientific Proteomics Facility for Disease Target Discovery at UCSF and the J. David Gladstone Institutes. Mass spectrometry data was assigned to human sequences and peptide identification and label-free quantification were performed with MaxQuant (version 1.5.5.1)(27). Data were searched against the UniProt human protein database (downloaded 2017). Statistical analysis was performed

using the MSstats Bioconductor package (25). Phosphoproteomic data was uploaded to the PhosFate profiler tool (28) (Phosfate.com) to infer kinase activity.

Multiplex inhibitor beads

Kinase chromatography, mass spectrometry and analytical processing were performed as described previously (29). Bait compounds were purchased or synthesized and coupled to sepharose. Cell lysates were diluted in binding buffer with 1 mol/L NaCl, and affinity purification was performed with gravity chromatography after pre-clearing. The bound kinases were stringently washed and then eluted with SDS followed by extraction/precipitation, tryptic digest and desalting. Liquid chromatography-tandem mass spectrometry (LC/MS-MS) was performed on a Velos Orbitrap (Thermo Scientific) with in-line high-performance liquid chromatography (HPLC) using an EASY-spray column (Thermo Scientific). Label-free quantification was performed with Skyline (30), and statistical analysis with Ms Stats (25).

Western blots and antibodies

Cells were lysed with RIPA and Complete protease inhibitors and PhosStop phosphatase inhibitors following standard techniques. Blots were cut to allow analysis of multiple proteins at different molecular weights, and stripping was performed with Restore Western Blot stripping buffer (Thermo Fisher), to allow analysis of phosphorylation and total expression. The majority of primary and secondary antibodies were obtained from Cell Signaling (Danvers, MA) as follows: AKT (Cell Signaling Technology Cat# 9272, RRID:AB_329827), Phospho-AKT S473 (Cell Signaling Technology Cat# 4060, RRID:AB_2315049), GAPDH (Cell Signaling Technology Cat# 2118, RRID:AB_561053), ILK (Cell Signaling Technology Cat# 3856, RRID:AB_2233861), MOB (Cell Signaling Technology Cat# 13730, RRID:AB_2783010). Phospho-MOB T35 (Cell Signaling Technology Cat# 8699, RRID:AB_11139998), PP2Ac (Cell Signaling Technology Cat# 2038, RRID:AB_2169495), Ribosomal protein S6 (Cell Signaling Technology Cat# 2217, RRID:AB_331355), Phospho-Ribosomal protein S6 S240/244 (Cell Signaling Technology Cat# 2215, RRID:AB_331682), RICTOR (Cell Signaling Technology Cat# 2140, RRID:AB_2179961), Phospho-RICTOR T1135 (Cell Signaling Technology Cat# 3806, RRID:AB_10557237), Yap (Cell Signaling Technology Cat# 12395, RRID:AB_2797897), Phospho-YAP S127 (Cell Signaling Technology Cat# 13008, RRID:AB_2650553). Actin (Sigma-Aldrich Cat# A2228, RRID:AB_476697), Flag (Sigma-Aldrich Cat# F3165, RRID:AB_259529) and Flag-HRP (Sigma-Aldrich Cat# A8592, RRID:AB_439702) were obtained from Sigma (St. Louis, MO), HBx (Abcam Cat# ab2741, RRID:AB_303266) and SMC5 (Abcam Cat# ab18038, RRID:AB_2192782) were obtained from Abcam (Cambridge, MA). Strep (Thermo Fisher Scientific Cat# MA5–17282, RRID:AB_2538748) was obtained from Thermo Fisher.

Quantitative Real Time PCR

RNA was extracted from cell lines with Trizol (Invitrogen). Reverse transcription was performed using the Superscript II RT kit (Invitrogen) with random hexamer primers (Roche). 18S and beta-actin were used as endogenous controls. All primers were generated

with the Primer3 online tool (http://bioinfo.ut.ee/primer3); sequences available on request. Quantification was performed using SYBR green labeling.

Immunohistochemistry

Analysis of mouse samples was performed on formalin fixed/paraffin embedded material with standard techniques and staining performed with anti-Ki67 (Thermo Fisher Scientific Cat# MA5–14520, RRID:AB_10979488; 1:150), followed by DAB development with Vectastain Elite ABC.

BrDU Incorporation

HUH7 or Hep3B cells were plated 1000 cells/well in black opaque bottom 96-well plates and BrdU cell proliferation kit protocol (Exalpha, Shirley MA) was followed. Briefly, cells were allowed to attach for 48 hours then BrdU at a final concentration of 10 μM was added for 2 hours. Cells were then fixed, washed and stained according to manufacturer's protocol. Final absorbance at 450 nm was read.

Vectors and cloning

We used the following vectors to engineer cell models: pHR-SFFV-dCAS9-BFP-KRAB (RRID:Addgene_46911) and pCRISPRia-v2 (RRID:Addgene_84832) was kindly provided by Luke Gilbert (UCSF). Gateway compatible pLVX-TetOne-Puro (RRID:Addgene_171123) was described previously (31), and adapted to hygromycin selection. HBV genes were PCR subcloned from the 1.3wt HBV construct (32), obtained from Addgene (RRID:Addgene_65462), and all human proteins used in AP-MS were obtained from the Orfeome v8.1 (33).

CRISPRi

Targeted CRISPRi analysis was performed following established protocols. Briefly, cells expressing dCas9-KRAB were sorted for BFP. dCas9-KRAB cells were then individually lentivirally infected with 3–5 sgRNAs against the gene target and selected with puromycin. Gene knockdown was confirmed by quantitative real time (QRT)-PCR, with sgRNA that failed to knockdown their target excluded from analysis. Proliferation of CRISPRi cells was performed on a ZOOM Incucyte over 120 hours. Area under the curve (AUC) analysis of cell count or confluence at each time point was developed and compared to cells transduced with a non-targeting control (NTC) sgRNA. expression correlation between proteins.

Data Availability Statement

The proteomics data have been deposited to the ProteomeXchange Consortium via the PRIDE partner repository with the dataset identifier PXD055366. The Reverse Phase Protein Array (RPPA) expression data from the TCGA Liver Cancer study analyzed in this study were obtained from the University of California, Santa Cruz Xena Genome browser at https://xenabrowser.net.

Code is on Github: https://github.com/adspit/HBV_HCC_interaction_inference.

Results

HBV-HCC interactome

We first performed affinity purification - mass spectrometry (AP-MS) to identify HBV PPIs (6) in the HUH7 HCC line. While this line is derived from a patient without co-morbid HBV infection, it can generate intact HBV virions from exogenous DNA (34,35), suggesting that it expresses all essential HBV-binding host proteins. Further, given that these cells were not exposed to HBV during tumor initiation, any HBV PPIs that exert anti-proliferative effects on HCC will not have been selected against. We used a 2X Strep epitope to tag and pull down each HBV protein, including Pol, HBc and HBx. In addition, we separately examined the secreted HBc variant e antigen (HBe) and short (SHB), medium (MHB) and long (LHB) isoforms of HBs (Fig. 1A). These were overexpressed individually in HUH7 HCC cells, with AP performed using streptavidin beads. Co-purifying human proteins were identified by MS and scored with MS interaction Statistics (MiST) software (20). Based on prior publications with subsequently validated viral interactomes, we defined a MiST score threshold of 0.75, which identified 145 total high-confidence PPIs (Fig. 1B; Table S1).

Functional analysis of the identified proteins with the Reactome database (36) revealed enrichment of proteins involved in pre-mRNA processing (HBc), nucleotide excision repair and mTOR signaling (HBx) and the unfolded protein response (HBe and LHB; Fig. 1C). The full map (Fig. 1D) included novel PPIs of HBV subunits with biologically significant host proteins including eIF4H and DDX3X (HBc) as well as Prohibitin 1 and 2 (LHB, SHB). It also included many known and suspected HBx interactions such as PRKAA1, PPP2CA, HDAC1, and the CRL4 E3 ubiquitin ligase complex. Selected PPIs were confirmed by AP-western (Fig. S1), chosen based on the results of the network propagation analysis below as well as their potential clinical actionability based presence of small molecule inhibitors. This interaction network provides an expanded view of the potential effects of HBV in HCC cells.

HBV significantly impacts gene mutation status in HCC

We next identified genes with differential mutational status relative to viral infection. We used Bayesian logistic regression to identify protein-coding genes with recurrent genetic alterations in The Cancer Genome Atlas (TCGA) HCC cohort (2) for which the alteration rate was significantly dependent on the presence of HBV or HCV infection (Fig. 2A). This strategy allowed us to evaluate the impact of the two hepatitis viruses on a broad spectrum of commonly and rarely mutated genes in HCC. We identified 70 genes with differential mutation based on viral status (p value <0.05, FDR < 20%; Table S2). The majority of differentially mutated genes had increased mutation frequency upon HBV viral infection (Fig. 2B). No statistically significant differences were observed in HCV-associated HCC compared to the remaining subsets. Notably, the tumor suppressors *TP53* and *MAP2K4* and the oncogene *GNAQ* were preferentially mutated in HBV+HCC, while the tumor suppressor *BAP1* was preferentially mutated in non-HBV-associated HCC. These data expand on our prior work (10) and confirm an impact of HBV on HCC genomes, but only provide partial insight into the ongoing role of HBV in HCC. Thus, we next pursued further investigation into direct effects of HBV.

Network model integrates oncogenic HBV protein and genetic interactions

To stratify PPIs based on the likelihood that they exert oncogenic effects, we used a network-based strategy to integrate HBV/host PPIs with differential HCC mutations, following the method established earlier for HPV (6). Point mutations and copy number aberrations that were less frequent in HBV-associated HCC (in comparison to HCV-associated and non-viral HCC) were used to identify mutations that might phenocopy HBV PPIs. This analysis followed the rationale that increased incidence of a mutation in the absence of HBV could indicate an important pathway in HCC that is directly modified by a PPI in HBV-associated tumors.

We applied statistical confidence measurements for our PPI and genomic data sets to the ReactomeFI network, a public catalog of >200,000 pathway relationships among human proteins, including PPIs, transcriptional regulatory interactions, and metabolic reactions. We used the framework of network propagation (36). Deviances reflecting significance of differential mutation and MiST scores reflecting PPI confidence were propagated separately across the network to generate a p value for each protein. Propagated p values were combined, resulting in a set of 61 network nodes with FDR < 0.1, indicating Proximity in ReactomeFI to HCC differential mutations and to HBV/host PPIs (Fig. 2C, Table S3). This set includes genes that did not meet our confidence threshold to be considered HBV PPIs but through network proximity and/or differential mutation meet the threshold of inclusion (Fig. S2A, shown in dark grey). This analysis allowed prioritization of a subset of the HBV/host PPIs and added related genes to their local networks. For HBc, interactions with SRPK1 and FUS were expanded to include KHSRP, ELAVL1 and PTBP1, giving a larger group of host factors with potential roles in HBV's known effects on splicing (37). Conversely, network propagation did not expand the set of PPIs for HBx. Instead, it allowed PPI prioritization based on cancer relevance, nominating COPS4, CUL4B, GART (a purine synthesis enzyme), PPP2CA and PRKAA1 key HBx effectors.

A key objective of this study is to identify HBV PPIs that may result in targetable vulnerabilities in HBV associated HCC. Given HBx's putative oncogenic role with anticipated effects on cell proliferation, we focused on the HBV PPIs that were also significant by network propagation and assessed their impact on cell proliferation with CRISPR interference with 5 independent sgRNA, using the essential gene Polo-like kinase 1 (PLK1) as a positive control. Knockdown of *CUL4B*, *PPP2CA* and *PRKAA1* increased HUH7 proliferation, while knockdown of *GART* and *COPS4* did not, showing a good concordance between our systems analysis and a relevant cancer readout (Fig. 2D). The Hep3B cell line is derived from a patient with HBV and can also support HBV replication (34), and was used for additional testing of the impact of HBx PPIs on cellular proliferation. In Hep3B, only PPP2CA sgRNA increased cell proliferation, with a lower relative change than observed for HUH7 as confluence rather than cell number was measured by real time microscopy (Fig. 2E). Thus, PP2A restrains proliferation in both HUH7 and Hep3B. We further found that increased cell numbers correlated with increased BrDU incorporation in HUH7 cells with *PPP2CA* knockdown (Fig. 2F). Knockdown was confirmed by QRT-PCR (Fig. S2B).

HBx physically remodels host PP2A complexes

With these HBx/host PPIs prioritized based on their impact on cell proliferation, we next assessed the mechanism by which HBx can act on these targets. While HBx interacts with components of the CRL4 E3 ubiquitin ligase (e.g. CUL4B) and its regulator the COP9 signalosome (COPS4), the impact of HBx to redirect CRL4 degrading activity towards the SMC5/6 complex is well described (12,13). Thus, we analyzed PP2A given its impact on proliferation in both HUH7 and Hep3B. The HBx/PP2A interaction has been previously demonstrated, but subsequent reports have shown different effects of HBx on distinct PP2A complexes (38–40). The PP2A holoenzyme consists of PP2Ac, the scaffolding subunit PP2AA (gene *PPP2R1A*), and one of >15 regulatory subunits. These subunits direct PP2Ac's substrate selection; several are tumor suppressors, including PPP2R4 and the PPP2R5 families (41). Thus, we hypothesized that HBx might alter PP2A's signaling effects via a mechanism that is sensitive to PP2A's interactions with its regulatory subunits.

Accordingly, we performed quantitative AP-MS with the PP2A catalytic subunit (PP2Ac, gene *PPP2CA*) in the presence or absence of HBx. The PP2A interactome showed significant changes in its interaction with regulatory subunits in the presence of HBx (Fig. 3A; Table S4). HBx expression resulted in reduced interaction between PP2Ac and PP2A regulatory subunits B alpha and delta (*PPP2R2A, PPP2R2D*), PP2A regulatory subunit B' delta (*PPP2R5D*), STRN3 and STRN4. STRN3 and STRN4 are components of the Hippo pathway regulating STRIPAK complex (42). HBx expression also resulted in reduced PP2Ac interaction with STRIPAK components STRIP1 and MOB4, as well as the DDR proteins RAD23A/B (Fig. 3B).

First, to understand the mechanism of these differential effects we used truncations to define the HBx/PP2Ac interaction surface and determined that HBx interacts with the first 108 amino acids of PP2Ac (Fig. 3C). This was modeled on the STRIPAK cryo-EM structure (43), showing that HBx binds to PP2Ac in a region that positions it to block binding of STRN3 and displace its associated complex components (Fig. 3D).

The PP2A holoenzyme is made up of PP2Ac, a scaffolding subunit and PP2A regulatory subunits, which direct PP2Ac's activity towards specific substrates. Thus, we used CRISPRi to prioritize the impact of different PP2A complexes on HUH7 and Hep3B proliferation. Strikingly, we find that while *PPP2R2D, PPP2R5D* and *STRN3* knockdown all increase HUH7 confluence, *STRN3* and *STRN4* knockdown increase Hep3B confluence (Fig. 3E-F). These data support our prior results that HBV/host PPIs tend to inactivate growth inhibitory mechanisms and nominate displacement of STRN3 from PP2A complexes as a key result of HBx/PP2Ac interaction.

HBx modulates HCC signaling by disrupting PP2A effects

The interaction between HBx and PP2A suggests a mechanism by which HBV can regulate HCC signaling. To understand HCC signaling in the context of basal HBx expression levels, we assessed a panel of liver cancer cell lines from HBV positive (n=11) and negative (n=5) patients. HBx gene expression was assessed by qPCR, with which we found that 8 of 11 HBV-associated HCC lines had detectable HBx levels (Table S5, Fig. S3A). As a

verification, we used PathSeq (10) to identify HBV sequences in RNA-Seq data available for 11 of these lines and found perfect concordance with our qPCR results. We used QRT-PCR to determine expression level of each PP2A regulatory subunit found to be displaced by HBx, and did not find a significant difference in expression level across the panel (Fig. S3A), nor did cells cluster by HBV RNA expression (Fig. S3B).

We then performed kinome profiling using Multiplex Inhibitor Beads coupled with mass spectrometry (MIB/MS) (29) to compare kinase expression and activity in HCC cells (Table S6). As MS detection is influenced by kinase expression levels, MIBs have somewhat reduced detection of kinases with low abundance but favor the measurement of kinases with poorly annotated targets. This dataset allowed us to assess whether endogenous HBx expression might alter PP2A activity. We studied this relationship by correlating expression levels of PP2A regulatory subunits whose presence in the holoenzyme is blocked by HBx (Fig. 3B) with signaling of their known targets. As expected, we observed consistent negative correlation between regulatory subunit expression and MIBs-determined kinase activity in non-HBx expressing cells, including PPP2R2D with CDK2, PPP2R5D with FAK, and AMPKA2 with STRN3 (Fig. 4A). STRIP1 is a STRN3 interacting protein that is present in MST1/2 regulating PP2A complexes (44). Expression of STRIP1 was significantly correlated with MST1/2 activity in non-HBx expressing cells (Fig. 4A), consistent with previous results (42). However, there was no correlation between PP2A subunit expression and activity of these kinases in HBx-expressing lines. These data suggested that HBx broadly disrupts signaling control by PP2A.

HBx effects on PP2A result in increased AKT and mTORC2 activation

We hypothesized that there may also be recurrently activated signals as a result of HBx effects on PP2A. Thus, we used global phosphoproteomics to assess changes in cellular signaling pathways in HUH7 cells upon HBx expression. Secondary analysis was performed with the Phosfate kinase attribution tool (28), which uses annotated phosphopeptides to identify kinases with altered activity in the presence of HBx. These data showed HBx-induced changes in motility, cell cycle/DNA damage, and stress and MAPK/PI3K pathways (Fig. 4B; Table S7,8), including a significant increase in AKT activity (7). We note that the AKT3 paralog is specifically identified as upregulated, although given the lack of clear differences in substrate selectivity between AKT1, 2 and 3 (45) it is possible that this is an analytical artifact. Pro-motility signaling such as Myosin light-chain kinase (MYLK) and p21-activated kinase 1 (PAK1) were also regulated. Notably, AKT exists in a feed-forward signaling loop with one of its key regulators, mTOR complex 2 (mTORC2), the rapamycin-insensitive complex that contributes to mTOR signaling, with known effects on metabolism and cell migration. As signaling from AKT and mTORC2 might be difficult to decouple using a signaling attribution tool, we also assessed our primary phosphoproteomics results for a recently annotated set mTORC2 targets from glioblastoma (46). Despite being from a distinct tissue type, we found this target set was significantly enriched in the phosphopeptides upregulated by HBx expression (Fig. S3C, $p<0.001$ by Chi-square test).

We tested these observations by western blot in HUH7. Strikingly, HBx overexpression increased activating phosphorylation of the essential mTORC2 scaffold RICTOR at T1135.

Importantly, the same effect was seen with the direct PP2Ac inhibitors LB-100 and okadaic acid (OA), with little additive impact of PP2A inhibition and HBx overexpression. While total RICTOR levels also change, this is consistent with a known stabilizing effect of this phosphorylation event (47). AKT phosphorylation was sufficiently low in HUH7 to be inconsistently detected by western blot, so is not shown. STRN3-associated PP2A can inhibit the Hippo tumor suppressor pathway via effects on the Hippo kinases MST1 and MST2 (42). Consistent with a loss of PP2A/STRIPAK activity, we found that HBx overexpression results in increased phosphorylation but reduced expression of the terminal Hippo target YAP, suggesting its downregulation by Hippo (Fig. 4C). We also note that OA treated cells express higher levels of HBx, although it is unclear if this is a direct effect of OA on HBx stability or on its expression from a plasmid.

Similar results were seen in HUH7 following *PPP2CA* knockdown, although we note that the sgRNA with more significant PP2Ac reduction was also associated with reduced RICTOR phosphorylation, potentially due to feedback effects due to chronic, rather than acute, PP2A downregulation (Fig. S3D). These findings were also tested in SNU-475, an HBx-expressing HCC line which expresses similarly high levels of STRIPAK subunits to HUH7 (Fig. S3B). Here, HBx overexpression did not dramatically impact Hippo signaling, as measured by MOB expression and phosphorylation. However, it dramatically increased RICTOR phosphorylation as seen above (Fig. 4C), with a more minimal effect on AKT phosphorylation (Fig. S3E). Suggesting that HBx effects on YAP are at least partially post-translational, we observed that MG-132 rescued the effects of HBx expression on YAP in HUH7 and Hep3B (Fig. S3F), and that HBx overexpression did not significantly alter YAP mRNA levels (Fig. S3G).

We also looked for recurrent signaling alterations across our MIBs data set, where PP2A regulatory subunit expression was more variable. As anticipated, the heterogeneity between cells in this larger collection resulted in relatively few consistently altered kinases based on HBx expression. These included the pseudokinase ILK, which is anticipated to still be detectable by MIBs via allosteric regulation of an ATP binding site (48), as well as the pro-inflammatory kinase RIPK2 and the pro-motility kinase TNK2 (Fig. 4D). Notably, AKT is relatively difficult to detect with MIBs (29) and was not identified in this analysis. ILK (49), RIOK2 (50), and TNK2 (51) have all been shown to activate mTORC2 output. Thus, even in cell models which lack high levels of STRN3, and thus are less likely to have significant activation of Hippo signaling, mTORC2 activation appears to be a recurrent event in the presence of HBx (see schematic, Fig. 4E).

mTOR Complex 2 regulates of YAP in HCC

Although signaling can be visualized as a series of linear kinase relays, many pathways exist in complex interconnected networks. Thus, the upregulation of the Hippo tumor suppressive kinase pathway raised the possibility that another aspect of HBx-induced signaling remodeling may exert an opposing effect to maintain YAP expression. Thus, we hypothesized that AKT and/or mTORC2 might influence YAP stability in HBx-expressing cell models. To address this possibility in a line without significant STRN3 upregulation, we shifted our experiments to the HBx+ Hep3B cells.

Consistent with results in HUH7, HBx overexpression and LB-100 treatment both reduced baseline YAP levels in Hep3B, although mTORC2 upregulation was limited. Cells were also treated with the allosteric AKT inhibitor MK2206 and the ATP-competitive mTORC1/mTORC2 mTOR inhibitor TAK-228 (sapanisertib). These data showed reduced YAP protein levels with each compound, with TAK-228 having the greatest effect. All effects were more pronounced in the presence of HBx (Fig. 5A), as seen above (Fig. 4C). As a parallel confirmation, we used CRISPRi to reduce expression of the PSK ILK, finding that it decreased YAP levels independent of HBx levels (Fig. S4).

We hypothesize that HBx accesses important cellular pathways rather than inducing them *de novo*, and thus that mTORC2 effects on YAP can be potentiated by either HBx or other factors signaling to these pathways. Thus, we next confirmed that TAK-228 treatment reduces YAP protein levels in the HBx-expressing cells SNU-182 and SNU-449 as well as the non-HBx expressing line SNU 423 (Fig. 5B), which has high levels of ILK activity based on the MIBs assay (Table S8). We confirmed that TAK-228's effect on YAP expression was due to mTORC2 inhibition by comparing the effects of the allosteric mTORC1 inhibitor everolimus, the Rapalink mTORC1 inhibitor (16) E-1035 and TAK-228 in SNU-182, observing that YAP levels are only reduced when mTORC2 is inhibited. Furthermore, this effect was sensitive to the proteasomal inhibitor MG-132, suggesting that mTORC2 acts on YAP degradation (Fig. 5C). Notably, MG-132 did slightly decrease pAKT and AKT levels, as has been previously described (52). Consistent with post-transcriptional YAP regulation, reduced mRNA expression of canonical YAP targets was also observed following TAK-228 treatment in cell lines, while YAP mRNA was not significantly changed (Fig. 5D).

To confirm this observation *in vivo* and validate the role of mTORC2 as a regulator of YAP in HCC, we tested the impact of *Rictor* deletion in an Akt/Ras-driven murine HCC model. Here, we found that Cre-mediated *Rictor* deletion resulted in longer survival compared to pT3 empty vector, with robust induction of aggressive tumors when Rictor was intact and improved survival in the absence of Rictor (Fig. 6A). When confirming *Rictor* deletion, we saw near elimination of YAP expression, as well as reduced but persistent Akt pS473 (Fig. 6B). Reduced YAP levels correlated with reduced proliferation by Ki-67 staining (Fig. 6C). These findings show that mTORC2 contributes to YAP regulation *in vivo* and again support its effect in the absence of HBx. These data suggest that the balance between Hippo and mTORC2 signaling control YAP expression in HCC. Consistent with this idea, we noted close correlation between levels of mTORC2 activation based on RICTOR pT1135 and YAP in HBV RNA+ and non-HBV RNA expressing specimens in TCGA. We also found that YAP and AKT pS473 were strongly inversely correlated in this data set (Fig. 6D), further supporting our finding that mTORC2 effects on YAP, are independent of AKT. Thus, rather than creating *de novo* signaling effects, HBx remodels a kinase network around the control of YAP levels, acting in parallel to augmenting an inhibitory signal (Hippo) that results in YAP phosphorylation and degradation as well as an activating signal (AKT/mTORC2) which maintains YAP expression even if it has been phosphorylated (Fig. 6E).

Discussion

This work describes the first complete HBV/HCC protein-protein and genomic interactome, and refinement of our network propagation strategy to identify cancer-relevant PPIs in genetically heterogeneous context of HCC. Our tiered analytical strategy allowed us to define remodeling of PP2A as an important HBV effector function, which appears to at least partially overcome a proliferative block applied by STRN3 containing PP2A complexes. Further, the increase in Hippo pathway activity resulting from HBx effects on STRN3/PP2A complexes may result in a dependency on mTORC2 function to maintain YAP protein levels. The significant alterations of PP2A function and the HCC kinome in the presence of HBx suggest that this may be one of several signaling dependencies emerging in the context of HBV infection. Further, mTORC2's maintenance of YAP expression in non-HBx-expressing specimens supports our model that HBV acts through cellular pathways that also support non-HBV-associated HCC.

This work advances the use of network strategies and multi-modality integrative models to study viral effects on cancer and reinforces the importance of protein interaction networks in defining disease-relevant genetic relationships (31,53). The mutations in non-HBV HCC that identified oncogenic HBV PPIs are not focused on a single oncogene or tumor suppressor, but rather occur across multiple members of a protein complex. By using network propagation, we were able to decode these relationships in an unbiased fashion and identify biologically meaningful relationships. This will likely broaden the utility of this strategy for the many other tumor associated viruses with indirect effects (54). Similarly, the integration of gene expression with proteomic data sets to assess the impact of HBx on PP2A interaction partners and downstream signaling allowed for the identification of a clear pattern of effects in multiple cell models.

Given the paucity of targeted therapy options for HCC, we focus here on signaling alterations that are driven by effects on PP2A. Viral disruption of PP2A function is common, with displacement of cancer-relevant regulatory subunits also seen in the context of the SV40 small T antigen (55), although HBx effects on PP2A do not appear to directly drive HCC proliferation. A broad array of viruses can influence PP2A activity in other ways to support their replication, including HCV which has been shown to express a PP2A regulatory subunit that can direct holoenzyme activity to inhibit inflammatory signaling (56). The remodeling of the PP2A complex by HBx decoupled it from the regulation of multiple cellular signaling pathways, most notably disrupting its inhibition of the Hippo tumor suppressor by STRN3/PP2A complexes and thus and decreasing YAP protein expression. This apparently growth inhibitory effect of HBx can be countered by mTORC2, which can maintain YAP protein levels by blocking its degradation. While prior studies have also shown that HBx can increase YAP mRNA expression (57,58), this effect of mTORC2 occurs even in the absence of HBx and is confirmed in mouse models and RPPA data from human HCC, suggesting it is a robust mechanism that may interact with the other mechanisms by which HBx augments YAP activity in HCC. We also note that mTORC2 has been shown to directly phosphorylate YAP at Serine 436. This may be the mechanism by which it stabilizes YAP (59), but we were unable to detect this phosphorylation by phosphoproteomics and there is no antibody publicly available to test it.

Limitations:

This study provides proof of concept for applying systems strategies to HBV and other viruses with indirect cancer promoting effects. One key potential limitation is the development of our AP-MS data in the HUH7 cell line, derived from a patient lacking HBV infection and previously used to develop the HCV PPI map (15). This line is one of three capable lines derived from patients without HBV that are nevertheless capable of supporting HBV replication, even though only a subset of lines derived from patients with HBV maintain HBV gene expression (Fig. S4) and replication (34). The loss of HBV gene expression in these latter lines suggests that in vitro culture adaptation may select against HBV replication potentially by downregulating interacting proteins.

HBx effects on PP2A and its impact on HCC signaling are just one of many potential HBV-induced effects on HCC biology, and we have focused on tumor cell intrinsic effects of HBV proteins, rather than those that may impact the HCC/microenvironment interaction. Similarly, while we provide valuable systems level data about HBV effects, some details are uncertain and may need to be validated as part of future studies (e.g., the identification of AKT3 as opposed to other AKT family members in phosphoproteomics, Fig 4B). Further, while our study highlights a relationship between HBx effects on PP2A and sensitivity to mTORC1/2 inhibitors, it does not provide evidence of preferential activity of mTORC1/2 inhibitors in HBV-associated HCC models. That analysis will require larger scale studies, such as the Phase 2 study of the mTORC1/mTORC2 inhibitor ATG-008 in HBV-associated HCC (NCT03591965) and may depend on co-occurrence of HBV infection and high level expression of STRN3. Similarly, additional study would be required to understand if HBx exerts oncogenic effects in *Rictor*$^{-/-}$ mice, and how YAP is regulated in that context.

In summary, our analysis provides comprehensive maps of the physical and genetic interactions between HBV and HCC, using computational methods to integrate these maps and nominate mechanisms by which HBV alters the behavior of HCC. Our validation of PP2A as one such mechanism supports the overall strength of our strategy, and future investigation can be used to assess a number of other targets of interest. Further, as large scale genomic datasets are analyzed in more depth, our estimate of the rate of direct viral infection of tumors is increasing to well over 10% (60,61). Our finding that HBV exerts ongoing effects on fundamental HCC processes encourages the application of this refined analytical strategy to the many other cancer-associated viruses.

Supplementary Material

Refer to Web version on PubMed Central for supplementary material.

Financial Support:

JDG was supported by an American Cancer Society Postdoctoral Fellowship, Conquer Cancer Foundation Young Investigator Award and Burroughs Wellcome Fund Career Award. KMS is supported by the NIH (RO1 A130699), and HHMI. RT was supported by the Hope Funds for Cancer Research (HCFR-21-05-05) and National Center for Advancing Translational Sciences (TR001871). AP was funded by the Joachim Herz Foundation with the Add-On Fellowship for Interdisciplinary Life Science. XC is supported by NIH grants R01CA136606 and R01CA190606. NJK and RKK were supported by the UCSF Program for Breakthrough Biomedical Research.

References

1. Sung H, Ferlay J, Siegel RL, Laversanne M, Soerjomataram I, Jemal A, et al. Global Cancer Statistics 2020: GLOBOCAN Estimates of Incidence and Mortality Worldwide for 36 Cancers in 185 Countries. CA Cancer J Clin 2021;71:209–49 [PubMed: 33538338]
2. Cancer Genome Atlas Research Network. Electronic address wbe, Cancer Genome Atlas Research N. Comprehensive and Integrative Genomic Characterization of Hepatocellular Carcinoma. Cell 2017;169:1327–41 e23 [PubMed: 28622513]
3. Totoki Y, Tatsuno K, Covington KR, Ueda H, Creighton CJ, Kato M, et al. Trans-ancestry mutational landscape of hepatocellular carcinoma genomes. Nat Genet 2014;46:1267–73 [PubMed: 25362482]
4. Gordan JD, Kennedy EB, Abou-Alfa GK, Beal E, Finn RS, Gade TP, et al. Systemic Therapy for Advanced Hepatocellular Carcinoma: ASCO Guideline Update. J Clin Oncol 2024;42:1830–50 [PubMed: 38502889]
5. Kim RD, Sarker D, Meyer T, Yau T, Macarulla T, Park JW, et al. First-in-Human Phase I Study of Fisogatinib (BLU-554) Validates Aberrant FGF19 Signaling as a Driver Event in Hepatocellular Carcinoma. Cancer Discov 2019;9:1696–707 [PubMed: 31575541]
6. Eckhardt M, Zhang W, Gross AM, Von Dollen J, Johnson JR, Franks-Skiba KE, et al. Multiple Routes to Oncogenesis Are Promoted by the Human Papillomavirus-Host Protein Network. Cancer Discov 2018;8:1474–89 [PubMed: 30209081]
7. Levrero M, Zucman-Rossi J. Mechanisms of HBV-induced hepatocellular carcinoma. J Hepatol 2016;64:S84–S101 [PubMed: 27084040]
8. Li Y, Tang ZY, Hou JX. Hepatocellular carcinoma: insight from animal models. Nat Rev Gastroenterol Hepatol 2011;9:32–43 [PubMed: 22025031]
9. Arbeit JM, Munger K, Howley PM, Hanahan D. Progressive squamous epithelial neoplasia in K14-human papillomavirus type 16 transgenic mice. J Virol 1994;68:4358–68 [PubMed: 7515971]
10. Lim HC, Gordan JD. Tumor hepatitis B virus RNA identifies a clinically and molecularly distinct subset of hepatocellular carcinoma. PLoS Comput Biol 2021;17:e1008699
11. Nassal M HBV cccDNA: viral persistence reservoir and key obstacle for a cure of chronic hepatitis B. Gut 2015;64:1972–84 [PubMed: 26048673]
12. Decorsiere A, Mueller H, van Breugel PC, Abdul F, Gerossier L, Beran RK, et al. Hepatitis B virus X protein identifies the Smc5/6 complex as a host restriction factor. Nature 2016;531:386–9 [PubMed: 26983541]
13. Murphy Christopher M, Xu Y, Li F, Nio K, Reszka-Blanco N, Li X, et al. Hepatitis B Virus X Protein Promotes Degradation of SMC5/6 to Enhance HBV Replication. Cell Reports 2016;16:2846–54 [PubMed: 27626656]
14. Sekiba K, Otsuka M, Funato K, Miyakawa Y, Tanaka E, Seimiya T, et al. HBx-induced degradation of Smc5/6 complex impairs homologous recombination-mediated repair of damaged DNA. J Hepatol 2022;76:53–62 [PubMed: 34478763]
15. Ramage HR, Kumar GR, Verschueren E, Johnson JR, Von Dollen J, Johnson T, et al. A combined proteomics/genomics approach links hepatitis C virus infection with nonsense-mediated mRNA decay. Mol Cell 2015;57:329–40 [PubMed: 25616068]
16. Rodrik-Outmezguine VS, Okaniwa M, Yao Z, Novotny CJ, McWhirter C, Banaji A, et al. Overcoming mTOR resistance mutations with a new-generation mTOR inhibitor. Nature 2016;534:272–6 [PubMed: 27279227]
17. Chen X, Calvisi DF. Hydrodynamic transfection for generation of novel mouse models for liver cancer research. Am J Pathol 2014;184:912–23 [PubMed: 24480331]
18. Reva B, Antipin Y, Sander C. Predicting the functional impact of protein mutations: application to cancer genomics. Nucleic Acids Res 2011;39:e118 [PubMed: 21727090]
19. Gelman A, Jakulin A, Pittau MG, Su YS. A Weakly Informative Default Prior Distribution for Logistic and Other Regression Models. Ann Appl Stat 2008;2:1360–83
20. Jager S, Gulbahce N, Cimermancic P, Kane J, He N, Chou S, et al. Purification and characterization of HIV-human protein complexes. Methods 2011;53:13–9 [PubMed: 20708689]

21. Shannon P, Markiel A, Ozier O, Baliga NS, Wang JT, Ramage D, et al. Cytoscape: a software environment for integrated models of biomolecular interaction networks. Genome Res 2003;13:2498–504 [PubMed: 14597658]
22. Choi H, Larsen B, Lin ZY, Breitkreutz A, Mellacheruvu D, Fermin D, et al. SAINT: probabilistic scoring of affinity purification-mass spectrometry data. Nat Methods 2011;8:70–3 [PubMed: 21131968]
23. Sowa ME, Bennett EJ, Gygi SP, Harper JW. Defining the human deubiquitinating enzyme interaction landscape. Cell 2009;138:389–403 [PubMed: 19615732]
24. Cox J, Mann M. MaxQuant enables high peptide identification rates, individualized p.p.b.-range mass accuracies and proteome-wide protein quantification. Nat Biotechnol 2008;26:1367–72 [PubMed: 19029910]
25. Choi M, Chang CY, Clough T, Broudy D, Killeen T, MacLean B, et al. MSstats: an R package for statistical analysis of quantitative mass spectrometry-based proteomic experiments. Bioinformatics 2014;30:2524–6 [PubMed: 24794931]
26. Budzik JM, Swaney DL, Jimenez-Morales D, Johnson JR, Garelis NE, Repasy T, et al. Dynamic post-translational modification profiling of Mycobacterium tuberculosis-infected primary macrophages. Elife 2020;9
27. Tyanova S, Temu T, Cox J. The MaxQuant computational platform for mass spectrometry-based shotgun proteomics. Nat Protoc 2016;11:2301–19 [PubMed: 27809316]
28. Ochoa D, Jonikas M, Lawrence RT, El Debs B, Selkrig J, Typas A, et al. An atlas of human kinase regulation. Mol Syst Biol 2016;12:888 [PubMed: 27909043]
29. Donnella HJ, Webber JT, Levin RS, Camarda R, Momcilovic O, Bayani N, et al. Kinome rewiring reveals AURKA limits PI3K-pathway inhibitor efficacy in breast cancer. Nat Chem Biol 2018;14:768–77 [PubMed: 29942081]
30. Schilling B, Rardin MJ, MacLean BX, Zawadzka AM, Frewen BE, Cusack MP, et al. Platform-independent and label-free quantitation of proteomic data using MS1 extracted ion chromatograms in skyline: application to protein acetylation and phosphorylation. Mol Cell Proteomics 2012;11:202–14 [PubMed: 22454539]
31. Kim M, Park J, Bouhaddou M, Kim K, Rojc A, Modak M, et al. A protein interaction landscape of breast cancer. Science 2021;374:eabf3066
32. Wang H, Kim S, Ryu WS. DDX3 DEAD-Box RNA helicase inhibits hepatitis B virus reverse transcription by incorporation into nucleocapsids. J Virol 2009;83:5815–24 [PubMed: 19297497]
33. Rual JF, Venkatesan K, Hao T, Hirozane-Kishikawa T, Dricot A, Li N, et al. Towards a proteome-scale map of the human protein-protein interaction network. Nature 2005;437:1173–8 [PubMed: 16189514]
34. Bhat SA, Ahanger IA, Kazim SN. Forthcoming Developments in Models to Study the Hepatitis B Virus Replication Cycle, Pathogenesis, and Pharmacological Advancements. ACS Omega 2023;8:14273–89 [PubMed: 37125123]
35. Ren S, Nassal M. Hepatitis B virus (HBV) virion and covalently closed circular DNA formation in primary tupaia hepatocytes and human hepatoma cell lines upon HBV genome transduction with replication-defective adenovirus vectors. J Virol 2001;75:1104–16 [PubMed: 11152483]
36. Fabregat A, Jupe S, Matthews L, Sidiropoulos K, Gillespie M, Garapati P, et al. The Reactome Pathway Knowledgebase. Nucleic Acids Res 2018;46:D649–D55 [PubMed: 29145629]
37. Duriez M, Mandouri Y, Lekbaby B, Wang H, Schnuriger A, Redelsperger F, et al. Alternative splicing of hepatitis B virus: A novel virus/host interaction altering liver immunity. J Hepatol 2017;67:687–99 [PubMed: 28600137]
38. He C, Qiu Y, Han P, Chen Y, Zhang L, Yuan Q, et al. ER stress regulating protein phosphatase 2A-B56gamma, targeted by hepatitis B virus X protein, induces cell cycle arrest and apoptosis of hepatocytes. Cell Death Dis 2018;9:762 [PubMed: 29988038]
39. Tsunematsu S, Suda G, Yamasaki K, Kimura M, Izumi T, Umemura M, et al. Hepatitis B virus X protein impairs alpha-interferon signaling via up-regulation of suppressor of cytokine signaling 3 and protein phosphatase 2A. J Med Virol 2017;89:267–75 [PubMed: 27459003]

40. Gong SJ, Feng XJ, Song WH, Chen JM, Wang SM, Xing DJ, et al. Upregulation of PP2Ac predicts poor prognosis and contributes to aggressiveness in hepatocellular carcinoma. Cancer Biol Ther 2016;17:151–62 [PubMed: 26618405]
41. Perrotti D, Neviani P. Protein phosphatase 2A: a target for anticancer therapy. Lancet Oncol 2013;14:e229–38 [PubMed: 23639323]
42. Shi Z, Jiao S, Zhou Z. STRIPAK complexes in cell signaling and cancer. Oncogene 2016;35:4549–57 [PubMed: 26876214]
43. Jeong BC, Bae SJ, Ni L, Zhang X, Bai XC, Luo X. Cryo-EM structure of the Hippo signaling integrator human STRIPAK. Nat Struct Mol Biol 2021;28:290–9 [PubMed: 33633399]
44. Tang Y, Chen M, Zhou L, Ma J, Li Y, Zhang H, et al. Architecture, substructures, and dynamic assembly of STRIPAK complexes in Hippo signaling. Cell Discov 2019;5:3 [PubMed: 30622739]
45. Johnson JL, Yaron TM, Huntsman EM, Kerelsky A, Song J, Regev A, et al. An atlas of substrate specificities for the human serine/threonine kinome. Nature 2023;613:759–66 [PubMed: 36631611]
46. Kalpongnukul N, Bootsri R, Wongkongkathep P, Kaewsapsak P, Ariyachet C, Pisitkun T, et al. Phosphoproteomic Analysis Defines BABAM1 as mTORC2 Downstream Effector Promoting DNA Damage Response in Glioblastoma Cells. J Proteome Res 2022;21:2893–904 [PubMed: 36315652]
47. Gao D, Wan L, Inuzuka H, Berg AH, Tseng A, Zhai B, et al. Rictor forms a complex with Cullin-1 to promote SGK1 ubiquitination and destruction. Mol Cell 2010;39:797–808 [PubMed: 20832730]
48. Fukuda K, Gupta S, Chen K, Wu C, Qin J. The pseudoactive site of ILK is essential for its binding to alpha-Parvin and localization to focal adhesions. Mol Cell 2009;36:819–30 [PubMed: 20005845]
49. McDonald PC, Oloumi A, Mills J, Dobreva I, Maidan M, Gray V, et al. Rictor and integrin-linked kinase interact and regulate Akt phosphorylation and cancer cell survival. Cancer Res 2008;68:1618–24 [PubMed: 18339839]
50. Read RD, Fenton TR, Gomez GG, Wykosky J, Vandenberg SR, Babic I, et al. A kinome-wide RNAi screen in Drosophila Glia reveals that the RIO kinases mediate cell proliferation and survival through TORC2-Akt signaling in glioblastoma. PLoS Genet 2013;9:e1003253
51. Mahajan K, Coppola D, Chen YA, Zhu W, Lawrence HR, Lawrence NJ, et al. Ack1 tyrosine kinase activation correlates with pancreatic cancer progression. Am J Pathol 2012;180:1386–93 [PubMed: 22322295]
52. Zanotto-Filho A, Braganhol E, Battastini AM, Moreira JC. Proteasome inhibitor MG132 induces selective apoptosis in glioblastoma cells through inhibition of PI3K/Akt and NFkappaB pathways, mitochondrial dysfunction, and activation of p38-JNK1/2 signaling. Invest New Drugs 2012;30:2252–62 [PubMed: 22367315]
53. Zheng F, Kelly MR, Ramms DJ, Heintschel ML, Tao K, Tutuncuoglu B, et al. Interpretation of cancer mutations using a multiscale map of protein systems. Science 2021;374:eabf3067
54. Tang KW, Alaei-Mahabadi B, Samuelsson T, Lindh M, Larsson E. The landscape of viral expression and host gene fusion and adaptation in human cancer. Nat Commun 2013;4:2513 [PubMed: 24085110]
55. Guergnon J, Godet AN, Galioot A, Falanga PB, Colle JH, Cayla X, et al. PP2A targeting by viral proteins: a widespread biological strategy from DNA/RNA tumor viruses to HIV-1. Biochim Biophys Acta 2011;1812:1498–507 [PubMed: 21856415]
56. Duong FH, Filipowicz M, Tripodi M, La Monica N, Heim MH. Hepatitis C virus inhibits interferon signaling through up-regulation of protein phosphatase 2A. Gastroenterology 2004;126:263–77 [PubMed: 14699505]
57. Zhang T, Zhang J, You X, Liu Q, Du Y, Gao Y, et al. Hepatitis B virus X protein modulates oncogene Yes-associated protein by CREB to promote growth of hepatoma cells. Hepatology 2012;56:2051–9 [PubMed: 22707013]
58. Wu Y, Zhang J, Zhang H, Zhai Y. Hepatitis B virus X protein mediates yes-associated protein 1 upregulation in hepatocellular carcinoma. Oncol Lett 2016;12:1971–4 [PubMed: 27602122]

59. Holmes B, Benavides-Serrato A, Saunders JT, Kumar S, Nishimura RN, Gera J. mTORC2-mediated direct phosphorylation regulates YAP activity promoting glioblastoma growth and invasive characteristics. Neoplasia 2021;23:951–65 [PubMed: 34343821]

60. Zapatka M, Borozan I, Brewer DS, Iskar M, Grundhoff A, Alawi M, et al. The landscape of viral associations in human cancers. Nat Genet 2020;52:320–30 [PubMed: 32025001]

61. Elbasir A, Ye Y, Schaffer DE, Hao X, Wickramasinghe J, Tsingas K, et al. A deep learning approach reveals unexplored landscape of viral expression in cancer. Nat Commun 2023;14:785 [PubMed: 36774364]

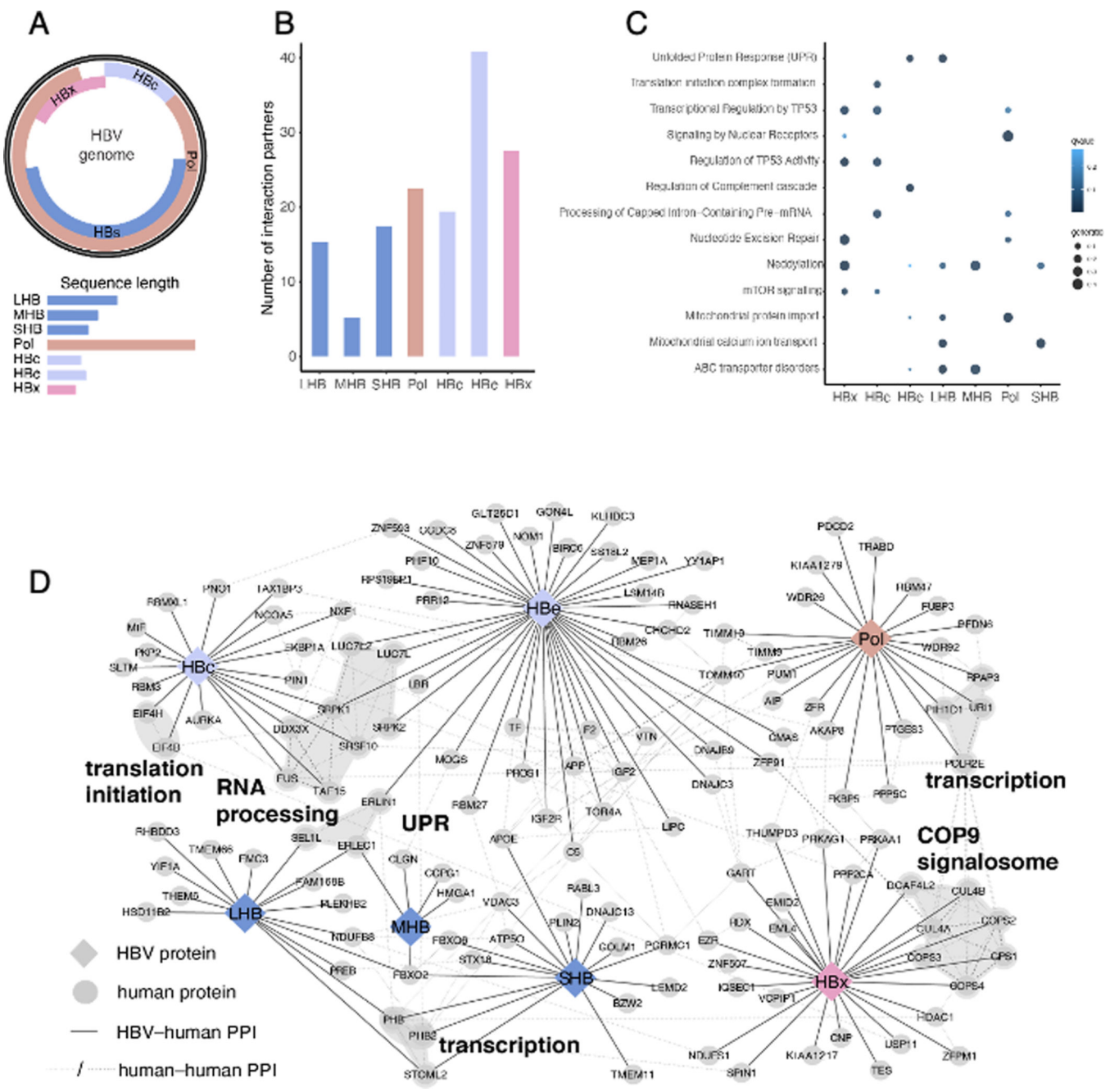

Figure 1: HBV-HCC protein interactome.

A) Map of the HBV genome with the outline of individual genes; genes are overlapping with distinct reading frames. Individual genes are shown below in linear format to indicate the length of each gene tested. **B)** Number of high-confidence PPIs for each HBV protein. **C)** Selected results of bioinformatic analysis of HBV PPIs using the Reactome pathway database. **D)** HBV interactome. Solid edges connect host proteins to the interacting HBV bait, while dashed lines show known human:human PPIs. Functional subsets and known protein complexes are investigator identified and designated with a grey background; n=2 biological replicates with 2 technical replicates per sample.

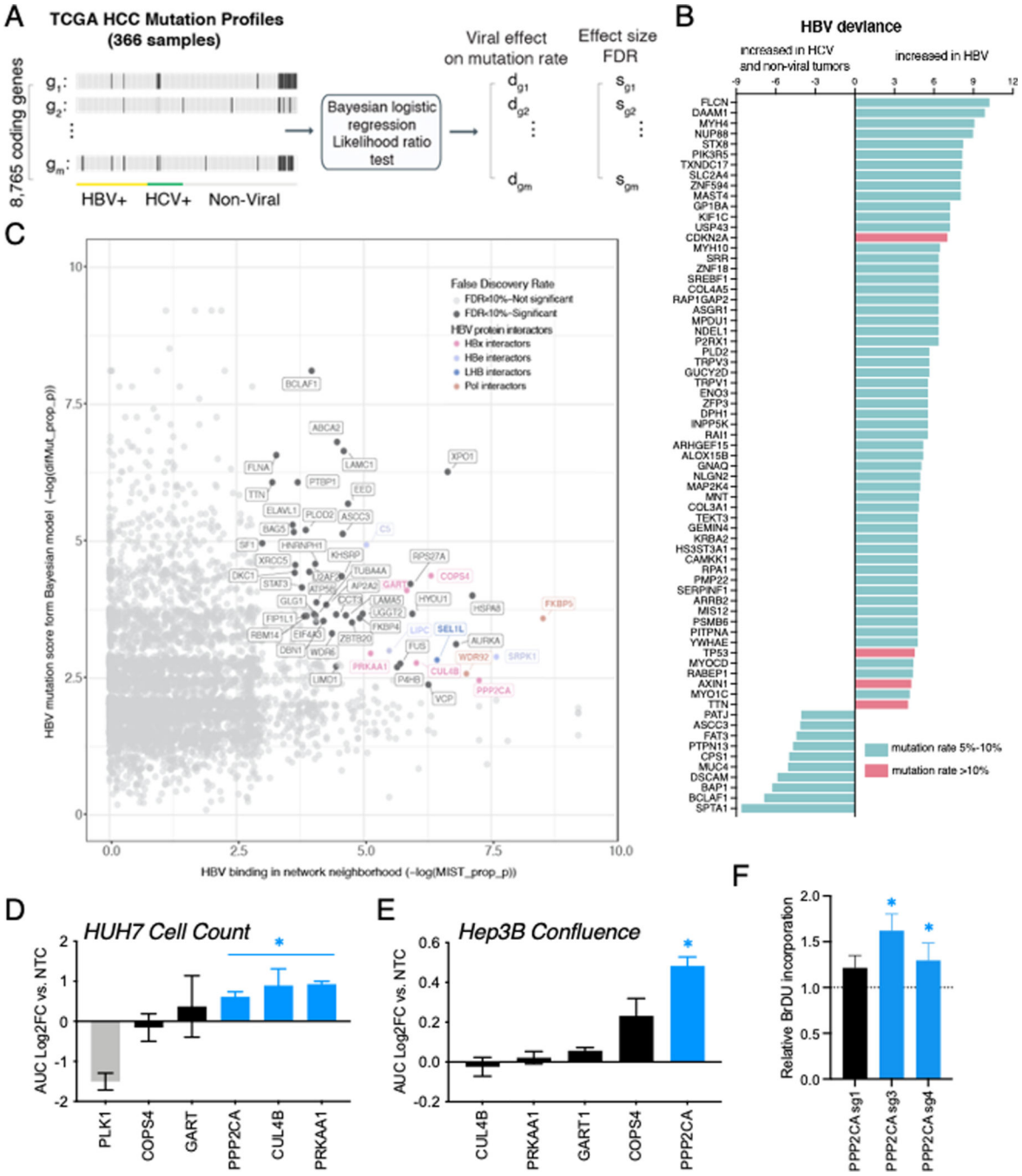

Figure 2: HBV-HCC genetic interactome.

A) Differential mutation analysis: Bayesian logistic regression was applied to 8,765 individual non-synonymous somatic mutations identified in the TCGA LIHC project to determine the predictive effect of HBV or HCV, or either infection, on the rate of each individual mutation. Viral status was determined based on clinical annotation. **B)** Deviance in HBV and mutation rate increased in HBV (positive) or increased in non-HBV vs. HBV (negative). All genes with a mutation rate above 5% in HBV-associated or non-HBV-associated HCC, with rates between 5–10% in blue and greater than 10% shown in red.

C) Scatter plot of network propagation distributed by the propagated p value for relative mutation vs. propagated p value for significance of HBV PPI. All nodes with FDR < 10% are labeled, and those that interact directly with an HBV protein are color coded by the HBV protein they bind. **D)** Analysis of HBx PPIs that are also significant from network propagation for effects on cellular proliferation measured by nuclear counting: HUH7 cells were engineered to express dCAS9-KRAB and then stably transduced with 4–5 sgRNA against each HBV PPI that reached significance in network analysis; PLK1 is included as an essential gene control. Effects on proliferation with real time microscopy over 120 hours are shown (* $p < 0.05$); n=3 biological replicates per sgRNA with a minimum of 3 technical replicates per sample. Area under the curve (AUC) analysis of cell count at each time point was developed and compared to cells transduced with a non-targeting control (NTC) sgRNA. **E)** Assessment of impact of HBx PPIs significant by network-propagation on proliferation in Hep3B. Analysis performed as in (D) above, with cell confluence measured in place of cell count. * $p < 0.05$, $n \geq 2$ biological replicates per sgRNA with a minimum of 3 technical replicates per sample. **F)** ELISA-based assessment of BrDU incorporation in HUH7 cells following PPP2CA knockdown. Results are from 2 biological replicates and a minimum of 3 technical replicates per sample normalized to NTC (*$p < 0.05$).

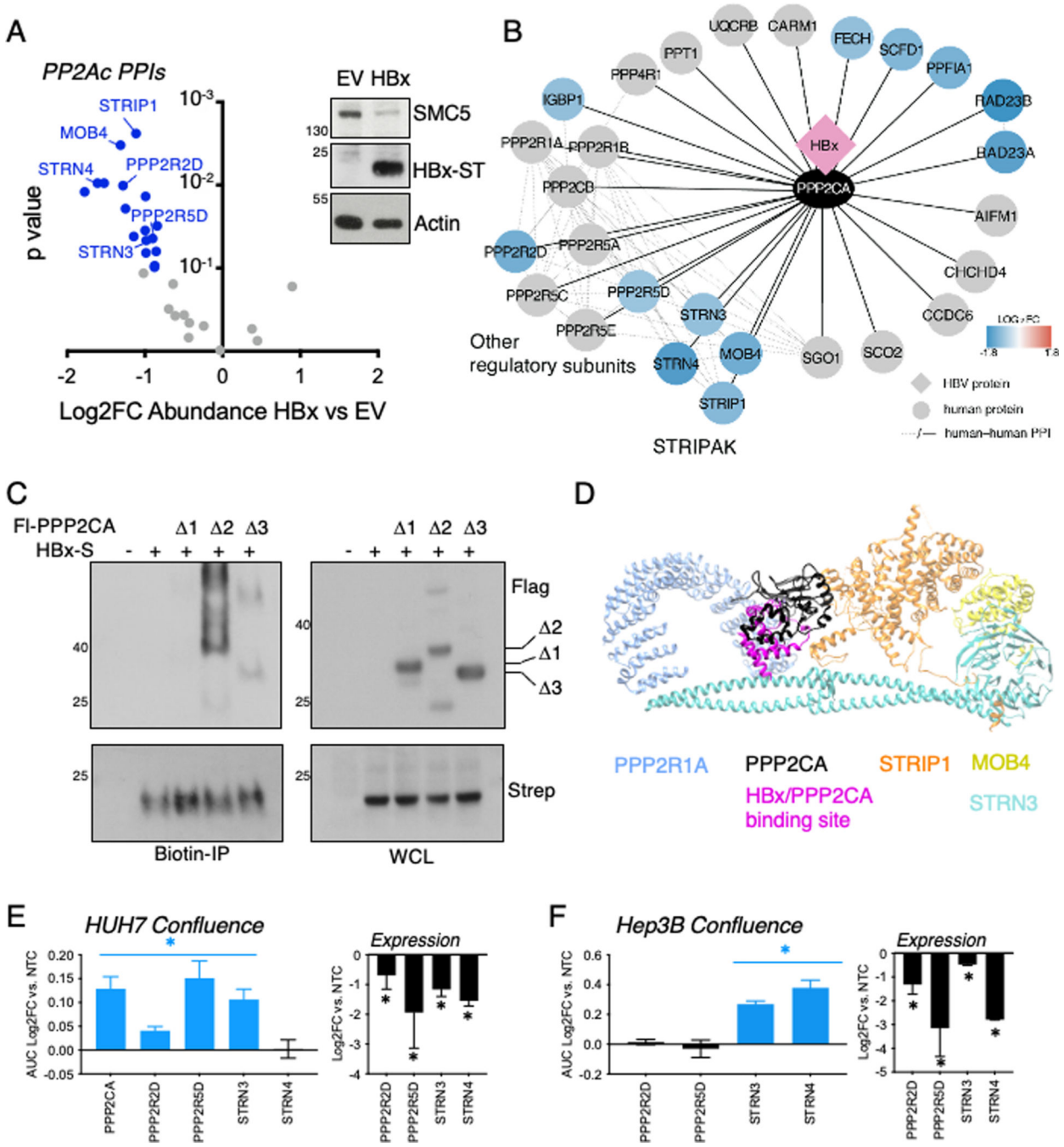

Figure 3: HBx remodels the PP2A holoenzyme.

A) AP-MS of the PPP2CA complex in HUH7 cells with co-transfection of Flag-PPP2CA and Strep-HBx vs. Flag-PPP2CA and empty vector (EV). High confidence PPIs are shown, with statistically significant changes in abundance in color; proteins of interest directly labeled. **B)** Cytoscape presentation of AP-MS results from (A). Proteins with significantly altered abundance are shown in color. There were no PPIs with increased abundance. **C)** Deletion mapping of the HBx/PPP2CA interaction with co-overexpression; for PPP2CA Δ1, aa1–108 are deleted: PPP2CA Δ2, aa109–189 are deleted; PPP2CA Δ3, aa190–310

are deleted. Biotin IP was used for complex purification and compared to whole cell lysate (WCL). HBx binding is lost by deletion of aa 1–108. **D)** Model of the HBx/PPP2CA interaction and its physical proximity to the PPP2CA/STRN3 interface overlaid onto the 7K36 cryo-EM structure. **E)** Impact of HBx-displaced PP2A subunits on HUH7 proliferation measured by confluence. HUH7 dCAS9-KRAB cells were stably transduced with ≥2 sgRNA against each PP2A subunit displaced by HBx, with PPP2CA knockdown shown as a benchmark. Effects on proliferation with real time microscopy over 120 hours are shown (* $p < 0.05$); n=2 biological replicates per sgRNA with a minimum of 3 technical replicates per sample. Area under the curve (AUC) analysis at each time point was developed and compared to cells transduced with a non-targeting control (NTC) sgRNA. QRT-PCR confirmed knockdown. **F)** Impact of HBx-displaced PP2A subunits on Hep3B proliferation as shown in **(E)**.

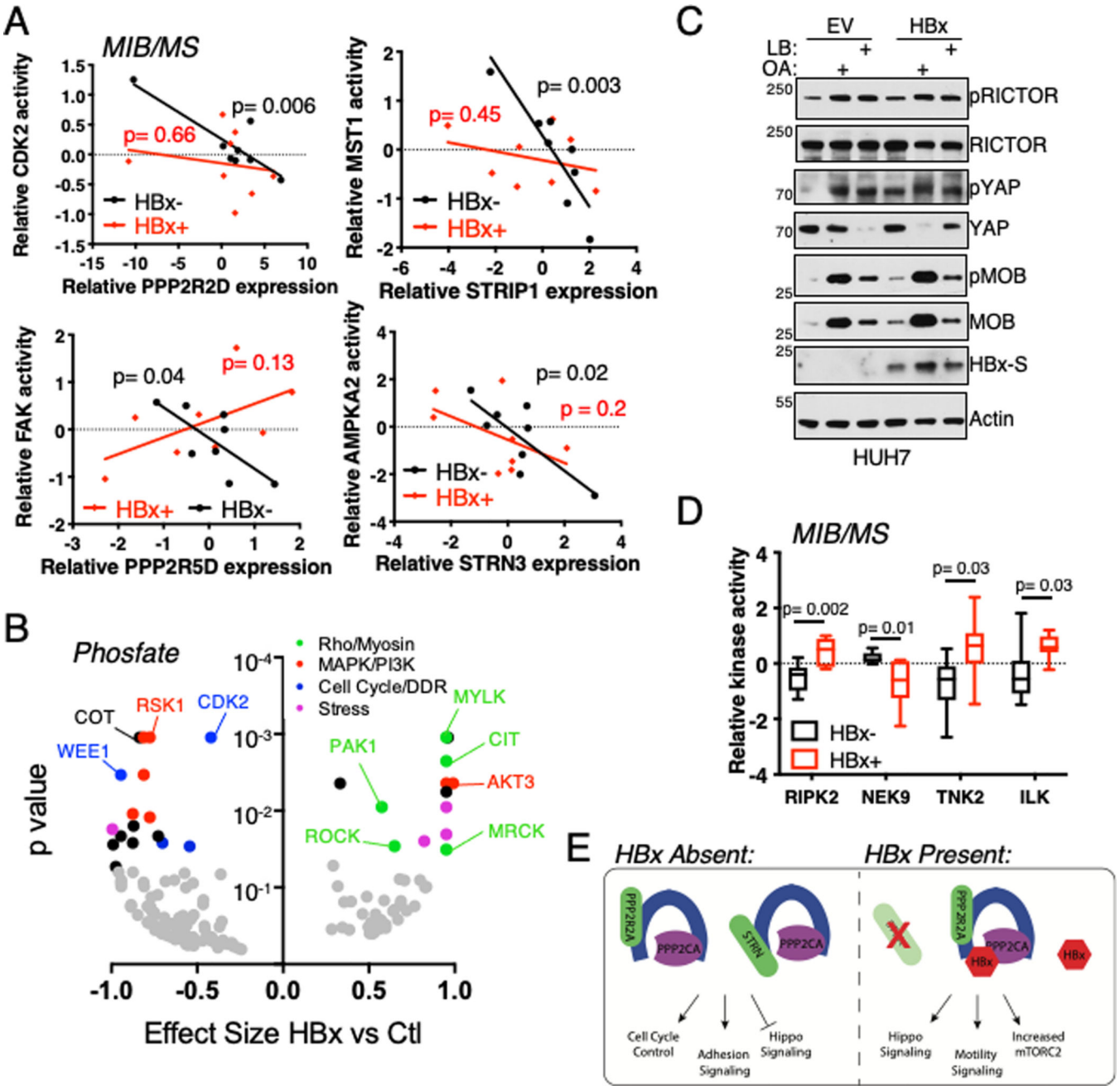

Figure 4: HBx alters HCC signaling by disrupting PP2A effects.

A) Correlation between PP2A component expression and individual kinase activity in a panel of 16 HCC lines, including 8 with detectable HBx mRNA expression; kinase activity determined using multiplex inhibitor beads (MIBs)/mass spectrometry (MS). In these cases, HBx expression decouples PP2A subunit expression from activation of it's PP2A complex's target kinase. **B)** Volcano plot of significant alterations in imputed kinase activation based on Phosfate analysis of global phosphoproteomics of HUH7 cells with doxycycline-induction of HBx for 48 hours. **C)** Effect of HBx expression on PP2A/STRIPAK target phosphorylation: HUH7 parental cells were transfected with pCDNA4 (EV) or HBx-ST

overnight and then treated with 50 nM okadaic acid (OA), 10 μM LB-100 (LB) or vehicle for 4 hours, resulting in altered phosphorylation and expression of RICTOR, MOB1 and YAP. **D)** Significantly altered kinase activity across our 16 HCC lines panel comparing cells with vs. without detectable HBx mRNA expression; kinase activity determined using MIBs/ MS; p values derived using t tests. **E)** Overall model for HBx effects on signaling: In the absence of HBx expression, PP2A function is determined by its typical upstream regulation mechanisms as well as the overall expression of its regulatory subunits (left). However, when HBx is present, its interaction with PPP2CA selectively disrupts PP2A function towards many targets, but does augment Hippo, mTORC2 and motility signaling (right).

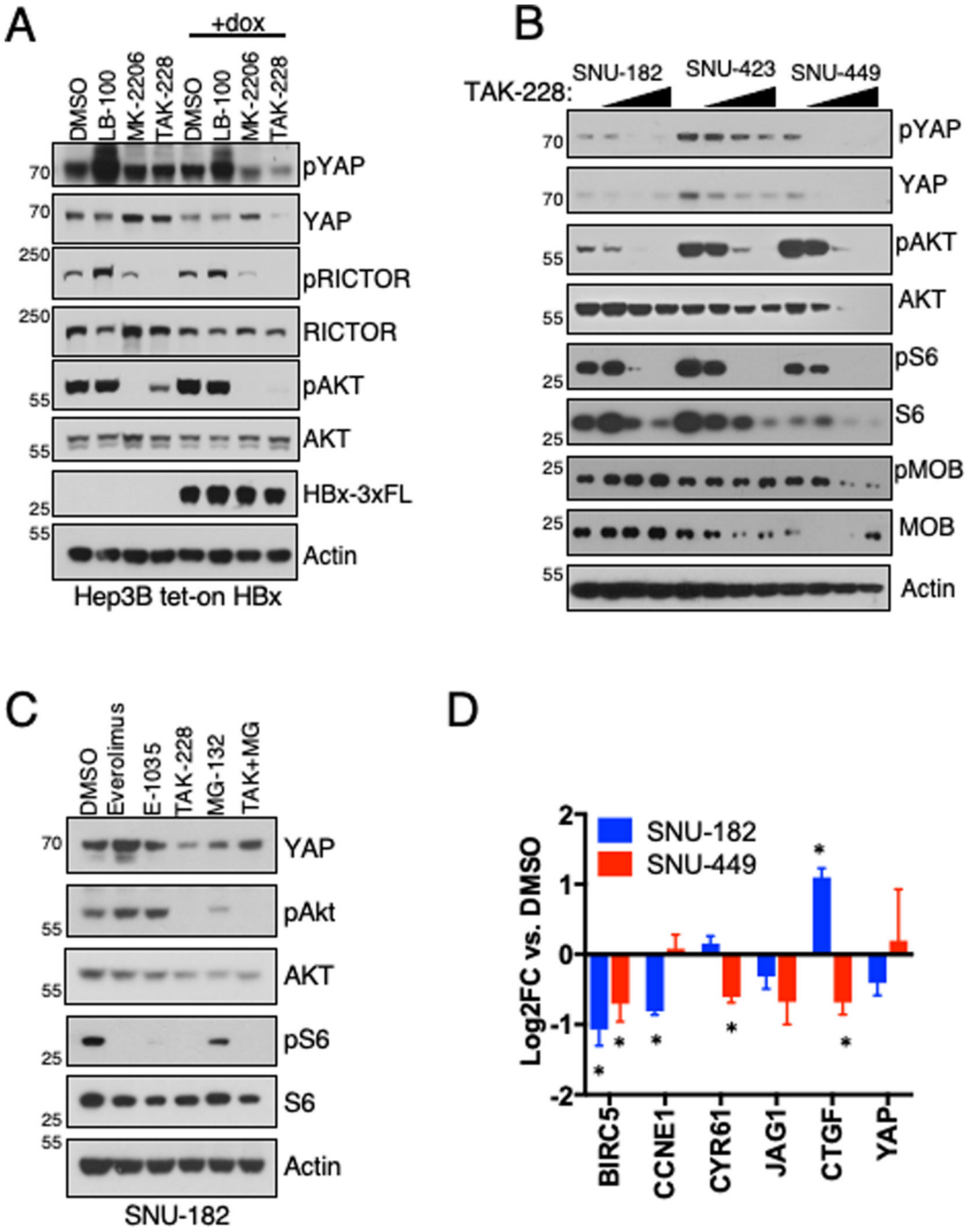

Figure 5: HBx stabilization of YAP via mTORC2.

A) Impact of HBx on regulation of YAP expression by AKT and mTOR. Hep3B cells with tet-inducible FL-HBx were treated with dox for 48 hours and then 1 mM MK-2206 or 100 nM TAK-228 or 10 μM LB-100 for 4 hours. n=2 biological replicates with 1 technical replicate per condition. **B)** Effect of DMSO or 20, 100 or 500 nM TAK-228 treatment for 24 hours on YAP expression in HBx+ SNU-182 and SNU-449 HCC lines or HBx- SNU-423 line assessed by immunoblot. n=3 biological replicates with 1 technical replicate per condition. **C)** Relative impact of mTORC1 and mTORC2 on YAP degradation: SNU-182

cells were treated for 4 hours with 100 nM everolimus, 100 nM of the Rapalink mTORC1 inhibitor E-1035, 100 nM TAK-228, 10 μM MG-132 or TAK-228+MG-132. n=3 biological replicates with 1 technical replicate per condition **D)** qPCR expression analysis of SNU-182 and SNU-449 cells of canonical YAP targets following 100 nM TAK-228 treatment for 4 hours, normalized to DMSO treated cells; * $p<0.05$ as determined by t-test; n=3 biological replicates with 3 technical replicate per condition.

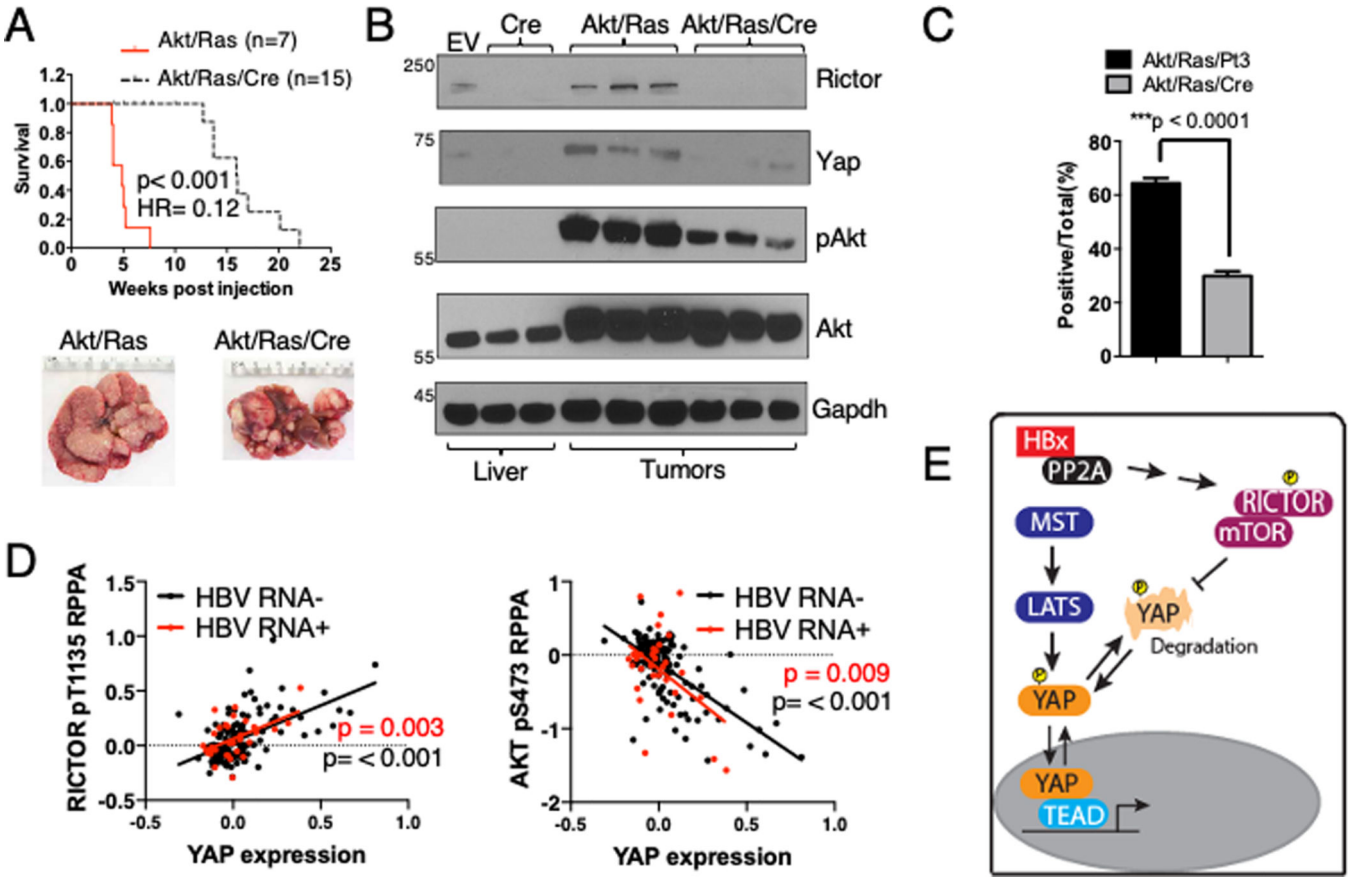

Figure 6: mTORC2 controls YAP in HCC *in vivo*.

A) Kaplan-Meyer survival analysis of *Rictor*$^{fl/fl}$ mice following hydrodynamic tail vein injection with Akt, Ras and empty vector or Akt/Ras/Cre. Akt/Ras/Vector mice were sacrificed at 5 weeks because of evident morbidity, and Akt/Ras/Cre sacrificed over time up to 22 weeks. Characteristic images of livers at necroscopy. **B)** Immunoblot analysis of Rictor, Yap, mTORC2 target Akt S473 phosphorylation in *Rictor*$^{fl/fl}$ livers transduced with empty vector or Cre, and then Akt/Ras or Akt/Ras/Cre tumors macrodissected at necroscopy. n=2 biological replicates with 3 technical replicate per condition. **C)** Quantified Ki-67 staining in Akt/Ras/Vector and Akt/Ras/Cre mice. **D)** Pearson correlation between RICTOR pT1135 or AKT pS473 and total YAP protein levels in HBV-associated and non-HBV associated HCC by RPPA from the TCGA LIHC project. **E)** Summary of model, showing parallel effects of HBx acting on PP2A-regulated cellular pathways to activate Hippo and mTORC2 signaling, resulting in maintained YAP expression.